Journal of Energy Storage 60 (2023) 106579

Contents lists available at ScienceDirect

Journal of Energy Storage

journal homepage: www.elsevier.com/locate/est

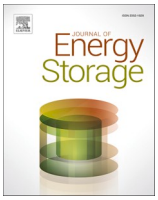

Review article

Meta-analysis of heat release and smoke gas emission during thermal runaway of lithium-ion batteries

Tim Rappsilber [a,*], Nawar Yusfi [a], Simone Krüger [a], Sarah-Katharina Hahn [b], Tim-Patrick Fellinger [a], Jonas Krug von Nidda [a], Rico Tschirschwitz [a]

[a] Bundesanstalt für Materialforschung und -prüfung, Unter den Eichen 87, 12205 Berlin, Germany
[b] Vereinigung zur Förderung des Deutschen Brandschutzes e.V., P.O. Box 4967, 48155 Münster, Germany

ARTICLE INFO

Keywords:
Lithium-ion battery
Thermal runaway
Cathode active material
Heat release
Smoke gas emission

ABSTRACT

Herein a meta-analysis of 76 experimental research papers from 2000 to 2021 is given about possible effects on the thermal runaway of lithium-ion battery cells. Data on the hazards of gas emissions and released heat are related to each other and differentiated by cell properties such as, cell geometry, cathode type or state of charge. Quantitative information on the total heat release in the range of 2.0–112.0 kJ Wh^{-1}, the peak heat release rate in the range of 0.006–2.8 kW $Wh^{-1}$and the smoke gas emission were extracted, normalized in terms of cell energy (Wh), combined in a data library and compared graphically. The total amount of gas emitted (3–48 mmol Wh^{-1}) as well as the released amount of carbon monoxide (1–161 mg Wh^{-1}) and hydrogen fluoride (2–197 mg Wh^{-1}) were investigated as a function of the state of charge and cell geometry. The analysis reveals that the measured values are significantly influenced by the types of calorimeters and smoke gas analyzers used as well as by the type of thermal runaway trigger. This meta-analysis can serve as an important basis for any risk assessment of lithium-ion batteries.

1. Background

In recent years the implementation of lithium-ion batteries (LIBs) increased exponentially. Due to their versatile design, LIBs have a broad performance range, which makes them broadly applicable. Typcially, LIBs offer high energy and high-power density at low weight and long life. Thus they are increasingly used in portable consumer electronics, battery electric vehicles and grid storage [1]. Consequently, the number of scientific studies investigating LIBs is also increasing. An important buzzword in connection with research on LIBs is the so-called Thermal Runaway (TR).

A TR often occurs when a LIB is subjected to a critical failure by means of mechanical, electrochemical and thermal failure [2]. These mechanisms often lead to unstoppable chain reactions that cause the cell temperature to rise significantly within a very short time, ultimately causing an abrupt release of energy [3–5]. The TR of LIB cells based on liquid electrolytes can be separated into three main stages:

Stage 1: If the heat generated by a critical failure cannot be dissipated, the temperature of the cell will continue to rise, potentially initiating a chain reaction of (mainly) exothermic reactions.
Stage 2: The solid-state electrolyte interphase is damaged at ≈80–100 °C, leading to an exothermic reaction between the electrolyte and (partially) charged anode. If the heat cannot be dissipated, the cell temperature consequently increases. A self-heating of ≈0.2 K min^{-1} is considered as onset temperature of the TR. The mechanical breakdown of the separator at ≈120–150 °C leads to an internal short circuit and a steep temperature rise due to large local currents. Above ≈180 °C, the cathode begins to decompose exothermically and release oxygen [6].
Stage 3: The resulting oxygen-containing atmosphere leads to a rapid, largely exothermic reaction with the electrolyte, causing a rapid temperature rise. A self-heating of ≥10 K min^{-1} is often defined as the TR starting temperature. The reaction is accompanied by enormous gas production, which can be accompanied by flame formation and/or an explosion.

Hence, two very important aspects for the characterization of the effects of a TR are the heat and the gases released. Corresponding

* Corresponding author.
E-mail address: tim.rappsilber@bam.de (T. Rappsilber).

https://doi.org/10.1016/j.est.2022.106579
Received 2 September 2022; Received in revised form 28 November 2022; Accepted 28 December 2022
Available online 8 January 2023

Nomenclature

C	Capacity, Ah
E	Energy content, Wh
m_{gas}	Total amount of gas emitted, mg
$\dot{m}_{gas}$	Gas emission rate, mg s^{-1}
n	Gas quantity, mmol
p_a	Ambient pressure, bar
Q	Total heat released, kJ
$\dot{Q}$	Heat release rate, kW
$\dot{Q}_{peak}$	Peak heat release rate, kW
t_{start}	Start of test time, s
t_{end}	End of test time, s
CF_4	Tetrafluoromethane
CO	Carbon Monoxide
CO_2	Carbon Dioxide
H_2	Hydrogen
HF	Hydrogen Fluoride
LiFSI	Lithium Bis(Fluorosulfonyl) Imide
$LiPF_6$	Lithium Hexafluorophosphate
PF_5	Phosphorus Pentafluoride
POF_3	Phosphorus Oxyfluoride
PVDF	Polyvinylidene Fluoride
AEGL	Acute Exposure Guideline Levels
ARC	Accelerating Rate Calorimeter
Bomb	Bomb Calorimeter
Comb.App.	Combustion Apparatus
Cone	Cone Calorimeter
CSBC	*Copper* Slug Battery *Calorimeter*
DSC	Differential Scanning Calorimeter
ERPG	Emergency Response Planning Guidelines
FTIR	Fourier Transform Infrared Spectroscopy
HeatFlux	Heat Flux Sensor
HRR	Heat Release Rate
GC	Gas Chromatography
GC–MS	Gas Chromatography − Mass Spectrometry
IC	Ion Chromatography
IDLH	Immediately Dangerous to Life and Health
IQR	Inter Quartile Range
LCO	Lithium Cobalt Oxide ($LiCoO_2$)
LFP	Lithium Iron Phosphate ($LiFePO_4$)
LIB	Lithium-Ion Battery
LMO	Lithium Manganese Oxide ($LiMn_2O_4$)
LNC	Lithium Nickel Cobalt Oxide ($LiNi_xCo_{1-x}O_2$)
NCA	Lithium Nickel Cobalt Aluminium ($LiNi_xCo_yAl_{1-x-y}O_2$)
NDIR	Nondispersive Infrared Sensor
NMC	Lithium Nickel Manganese Cobalt Oxide ($LiNi_xMnyCo_{1-x-y}O_2$)
PA	Paramagnetic Analyzer
PHRR	Peak Heat Release Rate
QEPAS	Quartz Enhanced Photoacoustic Spectroscopy
QMS	Quadrupole Mass Spectrometry
SBI	Single Burning Item Apparatus
SGE	Smoke Gas Emission
SOC	State Of Charge
Tewarson	Tewarson Calorimeter
THR	Total Heat Release
TR	TR
VSP2	Vent Sizing Package 2

experimental data published in literature show a large fluctuation range. For a general risk assessment that regards LIBs as a uniform energy storage device, it is indispensable to take into account valid data for the whole versatility of cell designs concerning both gas and heat release. A special focus should be placed on different – however, at the same time easily obtainable – battery parameters like cell geometry, cell size (geometrically or by means of stored electrical energy) or cell chemistry (e.g. cathode active material). It is therefore important to examine both aspects in detail. Active materials leading to significantly different performance parameters of LIBs are assumed to result in TR with different intensities. Thus, the cell chemistry will influence the hazard potential of the battery. Investigating the relation of different cell parameters to hazard potential is the core topic of this meta-analysis. We herein investigate if hazards caused by gas and heat release during TR can be reliable quantified by different methods and if those can be connected to rather easily accessible cell parameters. The authors hope that their analysis will provide insights into the maximum expectable hazards of particular cell types during a TR as another selection criterium for application. By combining and cross-referencing all currently available data, the analysis provides the reader with a comprehensive quantitative overview of the most studied TR effects of different LIB types.

2. General method

A systematic and selective survey of Web of Science, Google and Google Scholar was performed to identify original articles with experimental data on the heat release and gas emission during TR of LIBs. For the heat release the survey was carried out based on of following search terms:

- “Lithium-ion battery heat release rate TR”
- “(Automotive) lithium-ion battery heat release rate”
- “(Automotive) lithium-ion battery runaway”
- “(Automotive) lithium-ion battery calorimeter”
- “(Automotive) lithium-ion battery calorimetry”
- “(Automotive) lithium-ion battery fire test”
- “Electric vehicle battery Fire Test”
- “EV lithium-ion battery heat release”
- “Burning electric vehicle battery characterization”

As a result of this survey, 39 publications with concrete experimental values for the heat release rate or total heat release could be identified (June 2022). All experimental data were evaluated concerning the heat release rate and/or the total heat release as well as characteristics of the LIBs tested and experimental conditions.

For the second part dealing with the gas emission during TR following search terms were used:

- “Toxic emissions lithium-ion battery fire test”
- “Safety behaviour lithium-ion battery fire tests”
- “Gas amount released lithium-ion battery fire tests”
- “Gas analyses lithium-ion battery TR”
- “Vented gases lithium-ion battery TR”
- “FTIR and GC gas analysis lithium-ion battery”
- “HF, CO and CO_2 productions lithium-ion battery”

We included 37 references containing experimental data dealing with qualitative gas composition and quantitative amount of gas emission during LIBs TR (June 2022). All experimental values were evaluated regarding gas composition and/or total amount of gas emission. The test methods and LIBs characteristics were considered, too.

3. LIB nomenclature

The term lithium-ion battery is a collective term for a whole group of batteries based on different cell geometries and materials. One of the two main distinguishing features in this group, which are rather facilely retrievable, is the geometry of the cell. There are button cells, cylindrical cells, prismatic cells and pouch cells. Apart from button cells, which have received little attention in current LIB research, all the aforementioned cell types are addressed in this meta-analysis.

The compact cylindrical cells with high energy density are mainly studied in scientific publications. The investigation of space-saving and geometrically versatile pouch cells, on the other hand, is somewhat less common, but still much more frequent than the use of expensive prismatic cells with good cooling properties.

A second main distinguishing feature of LIBs, which can be obtained rather easily from commercial systems, is the cathode active material used. The cell chemistry largely influences the performance parameters, such as cell voltage, energy density, power ability and lifetime of a cell. The most common cathode active materials and their technical properties are compared in Table 1 [7]. In addition to the cathode active materials listed in the table, there are also some cell types comprising mixed cathode active materials, such as LMO + LNC, NMC + LCO or NMC + LMO.

In addition, there are also material variations in the electrolyte, separator and anode material of a lithium-ion cell, which can also influence the characteristics of the TR. However, there are currently only a few scientific papers dealing at least with the thermal stability of electrolytes [8,9]. For this reason, the population is far too low for statistical analysis. Following these parameters are not considered in this meta-analysis.

4. Creation of the data library

4.1. Data classification

This meta-analysis compiles specific quantitative data of 76 publications (June 2022). The listing of all available data sets in a data library should enable the interested reader to estimate the expected impacts of a LIB during TR. The data library includes the focal points *Total Heat Release* (THR) and *Peak Heat Release Rate* (PHRR) as well as the *Smoke Gas Emission* (SGE), all normalized in respect to nominal energy. A normalization in terms of cell weight is not consistently possible because of often withheld data. The values are categorized in the library according to different characteristics like *cell chemistry* (as per Table 1), *cell type* (pouch/prismatic/cylindric), *measuring apparatus* and *initiation method* of the TR. The *State Of Charge* (SOC), the *cell size* and *number of cells* per test were considered, too.

4.2. Hypotheses

The experimental data sets collected from the literature on heat release and smoke gas emission, cover a wide field in terms of measuring apparatus, initiation method of the TR and type of the tested LIBs. Based on these points, we formulate the following hypotheses:

a. The cathode active material influences both, the values of the heat release and gas emission.
b. The cell geometry influences both, the values of the heat release and gas emission.
c. The test method influences both, the values of the heat release and gas emission.
d. The initiation method influences both, the values of the heat release and gas emission.

If there can be stated an influence on one or more points, the second aim of this meta-analysis will be to quantify this influence.

4.3. Definition of the study variables

The online data library provided forms the basis for the diagrams shown in Section 4. To reach a comparability, normalized parameters were used to assess the hazard potential of LIBs with different cathode active materials. The three most important parameters used in the data library will be defined and briefly explained below.

4.3.1. Heat release rate

The HRR describes the intensity with which a fire releases energy. Thus, HRR is an essential parameter for predicting the fire propagation behavior to adjacent cells of the battery and other combustible materials. Other characterizing parameters of a fire, such as mass loss and smoke release, are directly related to HRR [10]. In most cases, HRR is calculated using a calorimeter via the oxygen consumption method. Only rarely, HRR is determined using heat flux sensors or mass loss values.

In this meta-analysis, the maximum measured HRR, the so-called peak heat release rate (PHRR), is reported always. The PHRR is the highest measured heat per time-step throughout the duration of the whole experiment and can be defined as:

$$\dot{Q}_{peak} = max.\left(\dot{Q}(t)\right) \quad (1)$$

Consequently, it depends on the duration of the time-interval chosen. Commonly, this should be in the range of a second. In this work, the maximum HRR is given normalized in terms of power per energy tested (kW Wh^{-1}), which is determined by dividing the PHRR by the energy stored in the tested device.

Table 1
Common cathode active materials of lithium-ion cells and their performance parameters [7].

Cell type	LCO	LMO	NMC	NCA	LFP
Cathode active material	Lithium Cobalt Oxide	Lithium Manganese Oxide	Lithium Nickel Manganese Cobalt Oxide	Lithium Nickel Cobalt Aluminium	Lithium Iron Phosphate
Nominal voltage, V	3,7	3,7	3,6/3,7	3,6	3,2/3,3
Volumetric energy density, Wh/l_{cell}	320–500	290–340	490–580	480–670	160–260
Gravimetric energy density, Wh/kg_{cell}	110–180	100–120	180–210	180–250	80–120
Typical discharge current, C	1–2	3–20	1–10	1–10	10–50
Lifetime, cycles	300–1000	1000–1500	500–1000	500–1000	2000–5000
Application ranges	High Energy (home appliance)	High Power (power tools, garden tools, medical application, military, vehicles)	High Energy + Power (home appliance, power tools, garden tools, medical application, vehicles, energy storage)	High Energy + Power (home appliance, power tools, garden tools, vehicles, energy storage)	High Power (home appliance, power tools, garden tools, medical application, military, emergency lighting, vehicles)

4.3.2. Total heat release

Another descriptor for hazard potential of a battery is the THR. Regarding a battery fire, the THR is the total energy released from the cell(s) throughout the complete process of the TR. Consequently, it is calculated from the integral of the measured HRR over the duration of the TR [10]. It therefore depends on the definition of start and end time of the test. Thus, the THR can be defined as:

$$Q = \int_{t_{start}}^{t_{end}} \dot{Q}(t)dt \quad (2)$$

As well as the HRR, the THR is given normalized in terms of total energy released per cell energy (kJ Wh^{-1}).

4.3.3. Smoke gas emission

In addition to the large amount of heat released during LIB fires, there are also hazards associated with the emission of smoke gases from defective LIBs. Particularly, in enclosed spaces where humans are present, the smoke gases emitted from a LIB during TR can pose a severe health hazard. In the event of overheating or fire, LIBs release, among others, large quantities of carbon monoxide (CO) and carbon dioxide (CO_2) [11], gases that are toxic in high concentrations. However, gases that are life-threatening even in small quantities, such as hydrogen fluoride (HF) gas, can also be produced [12]. In addition to the examples mentioned here, further flammable and toxic gases are released during TR [13–18].

The smoke gas emission values given in this paper describe the total emitted amount of gases from the cell(s) throughout the duration of a TR. It therefore depends on the definition of start and end time of the test. Thus, the smoke gas emission can be defined as:

$$m_{gas} = \int_{t_{start}}^{t_{end}} \dot{m}_{gas}(t)dt \quad (3)$$

To determine the smoke gas components and their concentrations, the smoke gases are analyzed using special analytical equipment. In this meta-analysis the concentration of toxic gases is normalized to cell energy and expressed in mg Wh^{-1} for specific gases and mmol Wh^{-1} for total amount of released gas.

The measurement of the gas concentration during a TR is a field of great importance in battery safety research. The hazard potential of the measured gases is evaluated using guidelines such "Acute Exposure Guideline Levels" (AEGL) [19], "Immediately Dangerous to Life and Health" (IDLH) [20] and "Emergency Response Planning Guidelines" (ERPG) [21].

4.4. Test methods and initiation mechanisms

The literature reviewed in this meta-analysis shows that a variety of test methods has been used to determine heat release and smoke gas emission during TR of LIBs. An overview of the most used test methods from 2000 to 2021 is given in Table 2, which also lists the standards on which some of the test methods are based. It turned out that the different test devices have different initial parameters, such as ignition source, ignition energy, ambient conditions, measuring method, measuring point, etc. Since those parameters influence the outcome the number of directly comparable measured values is limited.

Also, the terminology for test equipment used is not uniform. Test rigs that rely on the oxygen consumption method to determine heat release during TR of a LIB are named differently in different publications. In most cases these test rigs are referred to as "room calorimeter" [22], "combustion apparatus" [23–27] or "in situ calorimeter" [28–32]. To create a uniformly representable group from these different device notations, each of which is based on the same test method, the references just mentioned are classified into a group "combustion apparatus + oxygen consumption".

The publications evaluated mainly cover the years 2011 to 2021, as shown in Fig. 1.

4.4.1. Utilized test methods to determine the heat release

The most popular test methods to determine the heat release are the single burning item (SBI) test, the combustion apparatus (Comb.App.) and the cone calorimeter (Cone), as shown in Fig. 1. They have been widely used in publications from 2014 to 2019. The original work on thermal investigations to the best of our knowledge is published in 2000 by Venkatachalapathy et al. [35]. In this work, he extracted the material from $LiCoO_2$ and $LiNi_{0.8}Co_{0.2}O_2$ cathodes and investigated their heat release using the differential scanning calorimeter (DSC). The measured values of this method are specifically related to the studied material in pure form and cannot be compared with the values of other methods considering complete cells. The Tewarson calorimeter, also known as Fire Propagation Apparatus, has been used only by two research teams

Table 2
Applied test methods and devices for the determination of heat release and smoke gas emission during TR of LIBs.

Test method	Abbreviation	Measured value			Underlying standards		References dealing with
		HRR	THR	SGE			
Accelerating rate calorimeter	ARC	X	X		ASTM E 1981	[33]	[2,34–37]
Bomb calorimeter	Bomb	X	X		ASTM D2015	[38]	[39]
Burning chamber + Heat flux sensor	HeatFlux	X	X		ASTM E2684	[40]	[41]
Combustion apparatus + Oxygen consumption	Comb.App.	X	X		ISO 9705	[42]	[22–32,43,44]
Cone calorimeter	Cone	X	X		ISO 5660-1	[45]	[46–49]
Copper slug battery *Calorimeter* + Oxygen consumption	CSBC	X	X		ISO 5660-1	[45]	[50]
Differential scanning calorimeter	DSC	X	X		DIN EN ISO 11357-1	[51]	[36]
Vent sizing package 2	VSP2	X	X		N.A.		[52–54]
Single burning item apparatus	SBI	X	X	X	DIN EN 13823	[55]	[56–59]
Tewarson calorimeter	Tewarson	X	X	X	ISO 12136	[60]	[13]
					ASTM 2058	[61]	
					NFPA 287	[62]	
Fourier transform infrared spectroscopy	FTIR			X	ISO 19702	[63]	[8,12,13,16,17,44,57,58,64–70]
Gas chromatography - mass spectrometry	GC–MS			X	ASTM D4626	[71]	[14,15,17,18,66,70,73–77]
					ASTM D6420	[72]	
Ion chromatography + detector	IC			X	ASTM D4327	[78]	[64,65]
Multi-gas analyzer	MGA			X	N.A.		[28,43,49,58,79,80]
Nondispersive infrared sensor	NDIR			X	ASTM D3162	[81]	[8,44,57,68,76,82]
Paramagnetic analyzer	PA			X	IEC 61207-3	[83]	[44,58,76]
Quartz enhanced photoacoustic spectroscopy	QEPAS			X	N.A.		[75]
Quadrupole mass spectrometry	QMS			X	ASTM D2425	[84]	[75]

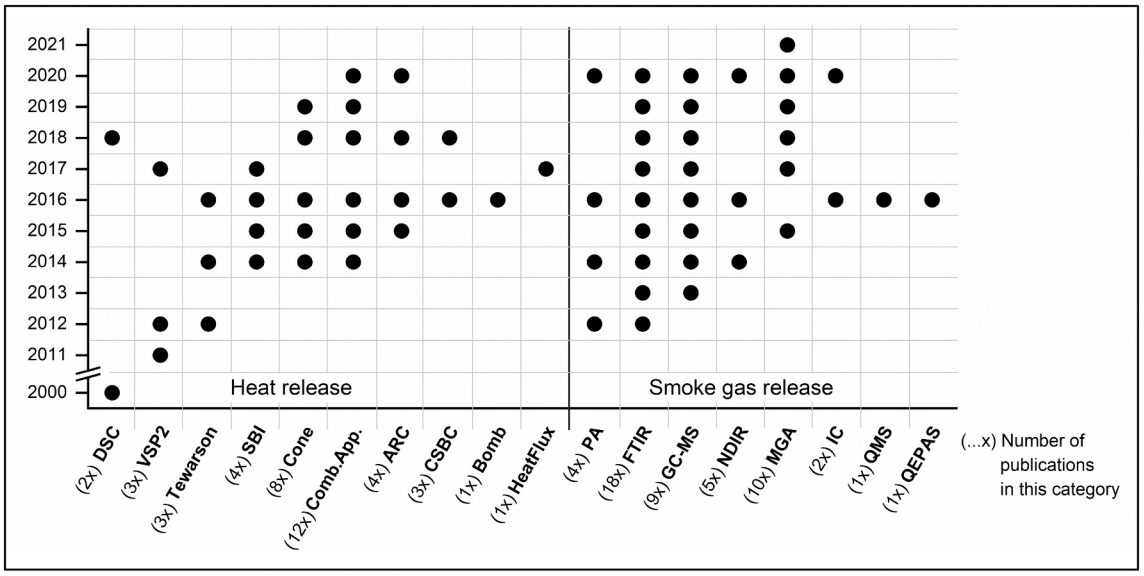

Fig. 1. Summary of utilized methods to determine the heat release (left) and to analyze the smoke gases (right) in the years from 2000 to 2021.

in all the literature analyzed. These are Ribière et al. [13] in 2012 and Lecocq et al. in 2014 [8] and 2016 [68]. Ouyang et al. [41] are so far the only ones who used a radiative heat flux sensor to determine the heat release rate of LIBs under overcharging. Another test method, the Vent Sizing Package 2 (VSP2), was applied by Duh et al. [52] and Jhu et al. [53,54] for their studies on thermal explosion hazards on 18,650 LIBs.

4.4.2. *Utilized test methods to analyze the smoke gas emissions*

The Fourier transform infrared (FTIR) spectroscopy and the gas chromatography (GC) were most used for toxic gas determination in publications from 2012 to 2020, as shown in Fig. 1. Another spectroscopic instrument, the nondispersive infrared (NDIR) sensor, was used for smoke analysis in the experiments by Eshetu et al. [8] and by Maloney [76]. Recently, it has been used by Cai et al. [82] to detect CO_2 within seconds after gas venting from LIBs. A paramagnetic analyzer (PA) has been used to determine the quantification of oxygen by Ribière et al. [13] in 2012. In addition to the previous methods to measure the gas emission, the gas-washing bottle technique was also used to determine the total fluorine (F_2) content in the gas, which cannot be measured by FT-IR. In 2017, first Larson et al. [85,86] used the gas-washing bottle as an additional measurement to validate the results of FTIR measurements and later, in 2019, Sturk et al. [64] used this technique for HF collection.

4.4.3. *Utilized initiation method to obtain a TR*

The influence of the different methods used to initiate the TR in the studies reviewed cannot be quantified within the scope of this analysis. However, each initiation method included in the present study, e.g. electric heating [22,24–29,31,32,39,41,48,50,87–90], radiant heating [13,23,30,32,46,49,91,92] or fire heating [56–59,93], are affecting the quantities of heat release and smoke gas emission differently, due to their different energy inputs. The exact amount of energy input significantly differs between different initiation methods, but also for experimental variants of the identical initiation method. For example, for the radiant heating method an increase of the incident heat flux from 10 kW m^{-2} to 75 kW m^{-2} was found to also significantly increase the measured surface temperature, PHRR, THR, mass loss and even in the CO or CO_2 production [46,92,94]. To precisely quantify the influence of different initiation methods on the intensity of a TR, many more studies on the effects of the initiation mode utilizing different LIB-types are needed.

5. Results

The total heat of combustion of each battery may be divided into the contribution of active components and the contribution of inactive components. Trends for the total heat of combustion for different tested cells may therefore be expected to be dependent on 1) the type of active material (cell chemistry) and 2) the ratio of active and inactive components. The absolute ratio of active-to-inactive material will significantly vary for the same cell geometry (e. g. cylindrical, pouch or prismatic cells). However, over the average of different ratios in different cell geometries, one can still expect a strong dependence of the ratio for different cell designs (e.g. high power vs. high energy cells).

5.1. *Heat release*

To obtain an overview of the measured values in literature for the maximum heat release rate and the absolute heat released from LIBs during a TR, all comparable measured values were recorded in Figs. 2 and 3. The measured values of all tests with lithium-ion single cells or cell bundles at a SOC = 100 %, depending on their cell design and cathode active material, were included in the diagram. Information on the type of set-up/test-method i. e., single burning item test [56–59], combustion apparatus [22–30,32], cone calorimeter [46–49,87–89,91,92], copper slug battery calorimeter [50,88,90], Tewarson calorimeter [13], accelerating rate calorimeter [35–37], heat flux radiometer [41], bomb calorimeter [39] or Vent Sizing Package 2 [52–54] are indicated by different colours. To be able to compare the measured values from tests with single cells and cell bundles, the data was normalized in respect to the nominal energy of the tested batteries.

Due to the sometimes closely spaced values, a clear numbering of each individual reference is unfortunately not possible. Therefore, the authors provide a table with the exact values for each reference in the supporting information of this publication.

In a second layer, box-whisker plots were generated for the corresponding data series, which provide information about the distribution of the measured values. A box (Inter Quartile Range, IQR) delimits the range in which the middle 50 % of all measured values of this measurement series are located. Within the IQR, a horizontal bar indicates the median and a white square outlined in black indicates the mean of all measured values. The whiskers include all measured values that scatter by 1.5 times the length of the IQR. Measured values that scatter outside this range are marked by a black square.

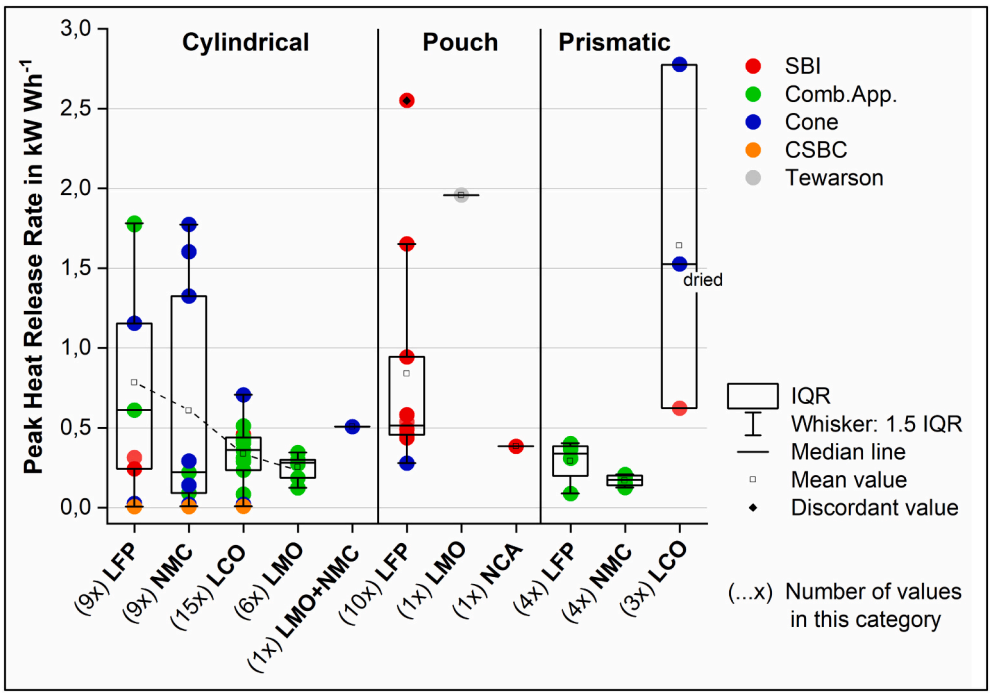

Fig. 2. Peak Heat Release Rate of cell(-bundle)s at SOC = 100 % depending on cathode active material and cell geometry.[1]
[1]Some of the values are not clearly recognizable as a separate entry because they differ only very slightly from the values of other entries and are therefore at the same level as the associated markers.

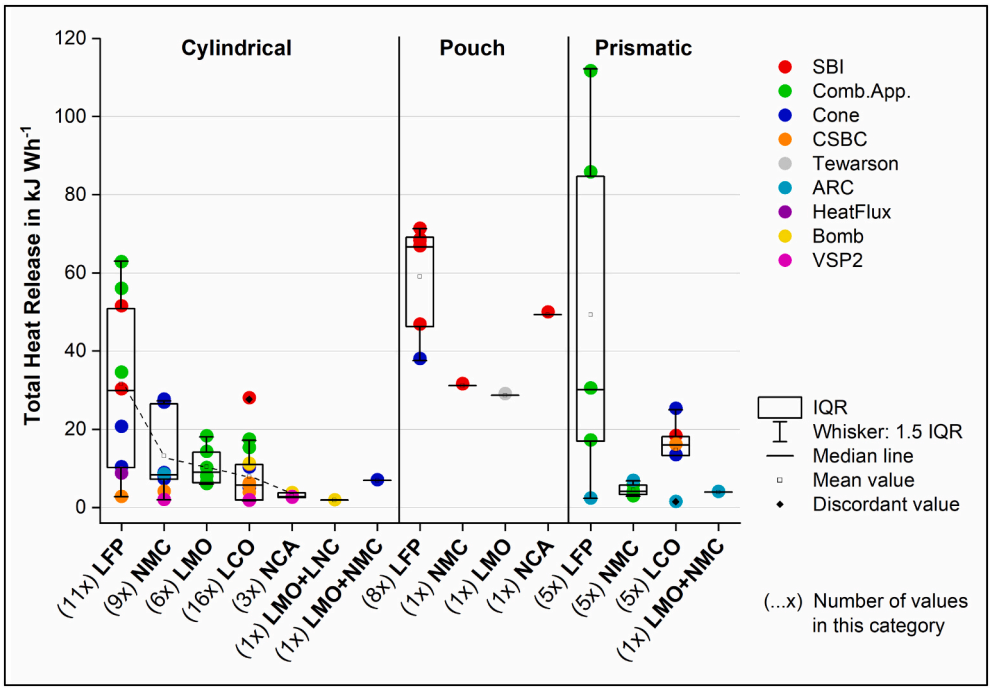

Fig. 3. Total Heat Release of cell(−bundle)s with SOC = 100 % depending on cathode active material and cell geometry.

Measured values of LIBs with varying SOC are not considered in detail in this section. Adding the factor *SOC* to the parameters *cathode active material*, *cell geometry* and *test method* limits the statistical population of each subsection in a way that no well-founded statements can be made with them.

However, such a SOC-dependent investigation of the THR can be carried out on the basis of LFP pouch cells. This investigation can be found in Section 5.3 *LFP - The most studied cathode active material.*

5.1.1. Peak heat release rate

More than 60 normalized literature values of all measured PHRR of cells or cell bundles, each with a SOC of 100 %, during a TR are graphically summarized and ordered by cell geometry and type of cathode active material (Fig. 2).

Most normalized PHRR values are in the range up to 0.7 kW Wh^{-1} (Fig. 2). Occasionally, however, values above 1.5 kW Wh^{-1} are also found in the diagram. The given data does not indicate a reason for those

large values. Neither a calorimeter type, a method for initiating the TR, a cathode active material, nor a cell design is frequently found among the high values. The number of cells used per experiment is also different. A particularly high total capacity of the tested batteries can also not be determined. However, it cannot be ruled out that these values are erratic.

5.1.2. PHRR of cylindrical cells

More than double as many results were found for cylindrical cells (15) as compared to pouch cells (6) and prismatic cells (6). The boxplot for cylindrical cells shows a clear gradation for all measured normalized PHRR mean values. The mean values (black outlined squares), drop noticeably among the first four cathode active materials ($\overline{PHRR_{LFP}} > \overline{PHRR_{NMC}} > \overline{PHRR_{LCO}} > \overline{PHRR_{LMO}}$). However, no correlation of this tendency to the respective volumetric or gravimetric energy densities of these cathode active materials (see Table 1) can be identified. Such a correlation is also not discernible in the categories pouch cells and prismatic cells. It should be noted that a value normalization in relation to the nominal energy of the tested batteries automatically increases the measured values of LFP cells due to their lower nominal voltage and their lower capacities. Normalization in terms of cell weight, which can only be implemented incompletely due to frequently missing data, would result in a different ranking among the mean values ($\overline{PHRR_{LMO}} > \overline{PHRR_{NMC}} > \overline{PHRR_{LFP}} > \overline{PHRR_{LCO}}$). The calculation of this ranking is based to a large extent on estimated weight values.

In contrast to the gradation of the normalized PHRR mean values shown, Miao et al. [95] who compared different LIB types for electric vehicle manufacturing, found a significantly different evaluation of the thermal properties of the cathode active materials. Their safety assessment in terms of thermal characteristics is as follows: LFP > NMC = LMO > NCA = LCO. Where LFP should be ranked safest and NCA equivalent to LCO most critical. According to Miao et al., one reason for this classification is that the phosphate in a LFP cell helps stabilize the electrode against the effects of overcharging. This gives the cell a higher thermal tolerance, which limits the thermal decay of the material, making it much less sensitive to TR [96]. The nickel contained in NMC and NCA cells provides high specific energy, but is known for its low stability, which is why these cell types are considered by Miao et al. to be less safe than LFP. NCA cells have higher specific energy and power density [96] and are thus considered more hazardous. LCO cells, which are equivalent to NCA cells in terms of safety, are very reactive and therefore have poor thermal stability.

If now the values of the different calorimeter types are considered, it can be stated that most of the values of the combustion apparatus are in the range of 0.08 kW Wh^{-1} [29] to 0.61 kW Wh^{-1} [30]. Only the green point of the combustion apparatus in the upper range of data series with cylindrical LFP cells consists (not apparent) of two entries with almost identical values: once reference [28] with 1.77 kW Wh^{-1} and once reference [30] with 1.78 kW Wh^{-1}. The clustering of values from combustion apparatus for the data series with cylindrical LCO cells resulted from two studies, both from Chen et al. [28,29].

The three entries in the lower range of the cylindrical LFP, NMC and LCO cells attributable to the copper slug battery calorimeter type are in a very narrow range of 0.005 to 0.006 kW Wh^{-1}. These values originate from [88] and represent the lower limit of all recorded measured PHRR values.

5.1.3. PHRR of pouch cells

In the middle section of the diagram, in which the investigations with pouch cells are recorded, it is noticeable that the SBI-test was frequently used for studies on that kind of cell type. Three of the four sources [56–59] dealing among others with the investigation of pouch cells in this apparatus are from Larsson et al. [56–58]. He always used the same setup for his investigations over the years, which positively influences the agreement of his results.

5.1.4. PHRR of prismatic cells

Only six publications could be found which deal with the PHRR investigation of prismatic cells. Four of these research [24,25,27,32] use the combustion apparatus to measure the PHRR. Their measured values are relatively close to each other with 0.13–0.40 kW Wh^{-1}. As with the cylindrical cells, the prismatic LFP cells also have slightly higher values than comparable NMC cells. The cone calorimeter measurements of Biteau and Nava [91] on prismatic LCO cells show two very different measured values. This difference is since they tested an untreated cell (2.78 kW Wh^{-1}) and a "dried" cell (1.53 kW Wh^{-1}), from which they removed the electrolyte before the investigation. They found that the dried cell released energy levels comparable to untreated LIBs with a SOC between 40 % and 50 %.

5.1.5. Total heat release

While the normalized PHRR (Fig. 2) is a descriptor for the kinetics of TR, the normalized THR relates to the (thermodynamic) energy content that can be released by TR. It shows the total energies released from the cell(s) throughout the complete process of a TR. The dependence of the THR for cell(-bundle)s with SOC = 100 % of the cell chemistry and cell type is shown in Fig. 3.

5.1.6. THR of cylindrical cells

The measured values of cylindrical cells recorded are based on 20 references and are mostly in the range up to 35 kJ Wh^{-1} (Fig. 3). However, four measured values are clearly above average showing values of 52–64 kJ Wh^{-1}. These are measurements from four different sources [28,30,31,58] on LFP cells of the 18,650 type. The three measured values recorded with the Comp.App. are from studies by Chen et al. [28,30,31], with the two highest measured values (56 and 64 kJ Wh^{-1}) coming from tests with single cells. The other two measured values of approximately 52 kJ Wh^{-1} are based on tests with a 4- and 5-cell bundle.

The range of cylindrical cells also contains the lowest measured values registered in the diagram. These values were recorded in test setups with bomb-, copper slug battery- and Vent Sizing Package 2 calorimeters.

In the area of the cylindrical cells, the boxplots behind them show a clear gradation of the THR mean values ($\overline{THR_{LFP}} > \overline{THR_{NMC}} > \overline{THR_{LMO}} > \overline{THR_{LCO}} > \overline{THR_{NCA}}$), which, however, differs in order from the gradation of the PHRR mean values from Fig. 2. In this case, too, no comprehensible correlation of this tendency with the respective energy densities of the associated cathode materials (see Table 1) can be discerned.

At this point it should be mentioned once again that the normalization applied here to the stored energy gives the LFP cells a high specific heat release per watt-hour due to their low energy content. Normalizing the values to cell weight rather than nominal energy would affect the classification of the heat release values of the various active cathode materials in a way that the LFP cells should be rated as one of the safest (see Section 5.1.1, *PHRR of cylindrical cells*).

5.1.7. THR of pouch cells

With six publications, only a few papers dealing with the THR of pouch cells could be found. The THR values reported of pouch cells with SOC = 100 % are in average higher than the average values of the other cell geometries as it can be observed in the middle section of Fig. 3.

The distribution of the measured values in the area of the pouch cells follows the same scheme as in Fig. 2. Here, it is again the publications of Larsson et al. [56–58] and Sturk et al. [59] whose investigations are based on the use of the SBI-test. Their results account for the majority of the measured values in this area.

When considering the THR values as a function of the cell geometries, it is noticeable that pouch cells release more heat on average over the duration of the test than the other cell geometries listed. A factual

based statement cannot readily be made about the reasons for this behavior. One possible explanation could be the high specific energy density that pouch cells can achieve with their construction of ultra-thin layered films <100 μm thick [97]. In addition, pouch cells are encased with an aluminium-plastic composite film that has a cell component-resistant polyolefin coating on the inside and an environmentally resistant polyamide coating on the outside [97,98]. These plastic coatings provide an additional fire load in case of combustion, which may also contribute to the higher total energy release. In their study on fire-induced hazards of Li-ion pouch cells, Ribière et al. [13] conclude, that the THR of a cell fire can be estimated by simply adding the contributions of all polymers and electrolyte combustion heats. Accordingly, 50 % of the combustion heat of the tested pouch cells originates from the polymers contained in the cell.

It is noticeable that LFP cells have the highest THR values for all the cell geometries recorded in the diagram. For cylindrical and pouch cells, the mean THR values of the LFP cells are twice as high as those of the NMC cells. A possible explanation for this is presented by Sturk et al. [59] just like Biteau and Nava [91], according to which the electrolyte contained in the cell, rather than the cathode material, is the main factor responsible for the thermal energy released during combustion. The cathode material, which is commonly used to evaluate the safety parameters of a LIB, is not always determinative of the behavior of a cell during TR, he said. He based this on the research of Huang et al. [99] and Wang et al. [100], who found that the electrolytes in a cell contain more combustible energy per unit mass than the Li-ion battery cell offers in electrical energy. In addition, the flame retardants and additives used by the cell manufacturers also have an impact on the heat generation during TR according to Xiao et al. [101]. In conjunction with his measured values of LFP and NMC cells, which have a similar distribution as the LFP and NMC values in Fig. 3, Sturk et al. theorizes that the heat released from a LIB in the event of a fire, is related to the cell volume and thus the chemical constituent content rather than the specific electrical energy density of the cathode material [59].

5.1.8. THR of prismatic cells

The data of prismatic cells from a total of 8 different references are mainly in the range up to 25 kJ Wh^{-1}. However, the three highest measured values for THR (85, 86 and 113 kJ kW^{-1}) are also found in the area of the prismatic cells. They originate from two studies on 50 Ah LFP batteries, whose energy release was determined in a Comb.App. using the oxygen consumption method. In [24], a 50 Ah battery is used. In [25], the battery under study is composed of 5 pieces of 10 Ah cells. This composed battery pack reaches 113 kJ Wh^{-1}, the highest measured value recorded in the plot. Both investigations are from the University of Science and Technology of China, Hefei.

5.2. Smoke gas emission

The collected research results on smoke gas emission are related to the study of thermal properties of LIBs using heaters and gas analyzers. As in the studies on the heat release from LIBs, cylindrical cells are also often used in the studies on smoke gas emission. A precise distribution of cell types among various research papers can be found in the additional table provided online with all collected data on smoke gas emission.

Due to the high energy density of a battery and the chemical properties of the electrolyte, the reactions triggered during TR within the cell can result in cell temperatures of over 1000 °C [14,15]. In addition to a high amount of heat the TR reactions produce large volumes of carbon monoxide (CO), hydrogen (H_2) and carbon dioxide (CO_2) thus making the gas flammable and potentially toxic [95].

From a series of tests performed by Golubkov et al. [15] on 23 NCA and LFP-based 18,650 LIB cells, it is found that the type of cathode material has a great influence on the released gases under TR conditions. Thus, NCA-based cells showed a severe TR behavior. During the experiments, they reached temperatures in the range of 739 °C to 1075 °C depending on the SOC and released up to 317 mmol of gas. Under identical conditions, LFP-based cells reached only half the temperature and a gas emission of 61 mmol. The gas composition of these two cell types were mostly dependent on the cathode material. Thus, NCA cells produced more CO and H_2 than LFP cells. The SOC also influenced the gas composition. Low-charged cells produced mainly CO_2 whereas higher charge states resulted in larger amounts of CO and H_2. One possible explanation is the Boudouard equilibrium, which states that the fraction of CO/CO_2 is temperature dependent. According to this, at high temperatures, which are to be expected during the TR of cells with high SOC, a reduction of CO_2 with carbon to 2 mol CO takes place.

5.2.1. CO production

It is well known that CO is a respiratory poisonous substance, that is easily absorbed through the lungs and cuts off oxygen transport in the human organism, threatening death by suffocation. The colorless, odorless and tasteless properties of the gas make it particularly insidious. Further on, it forms an explosive atmosphere in a very wide concentration range (11–76 %) [102]. For these reasons, it is worthwhile at this point to take a closer look at the release of CO from LIBs, during TR.

In the following section, the influence of cell geometry and SOC on CO production is determined. To illustrate the relationships, the data collected in the literature articles were recorded and systematically compared in Fig. 4. Again, the measured values used were normalized to the nominal energy of the batteries tested. As in the previous figures, a box-whisker plot was added in a second layer, which provides more detailed information on the distribution of the measured values.

5.2.1.1. CO production of cylindrical cells. Compared to pouch cells, cylindrical cells have a relatively narrow range of CO values from 1 to 45 mg Wh^{-1} over all SOCs. Golubkov et al. [15] present a couple of the few series of measurements in this field which investigate one and the same cell type under identical conditions at SOC-levels from 0 % to 100 %. The essential data of these test series with cylindrical LFP and NCA cells are part of Fig. 4. When looking at them, it is noticeable that both the NCA and LFP cells show higher CO emissions with increasing SOC. Golubkov et al. assume that the smoke gases are not fully detected by the gas chromatography system when the cells are discharged and that this is the reason for the very low measured values, especially for NCA cells. One reason for this could be the barely detectable exothermic reactions in discharged LFP or NCA cells. In both cell types, the initial burst plates of the cell housings open in the discharged state, whereupon a uniform gas emission takes place over the duration of the cell heating. The situation was similar for slightly charged cells (SOC = 25 %). Only at a SOC of 50 % or more, pronounced TR reactions with stronger smoke gas emission were recorded [15].

All other measured values of cylindrical cells are individual measurements, or series of measurements, which do not extend over the entire cell voltage range. Since it can be assumed that the different test methods limit comparability, no behavioral predictions can be made from these data as a function of the SOC. Nevertheless, they help to strengthen the validity of the CO production averages in dependence on the SOC. The boxes around all measured values show that the mean values of CO production increase with increasing SOC. One reason for this could be the increasing amount of combustible gases and oxygen accumulating inside the cell during TR. Chen et al. [28] and Wang et al. [103] referred that large amounts of gas accumulate inside the cell at higher states of charge. Wang et al. [103] state that at the moment the burst plates ruptures, the escape velocity of these gases is so high that they are not ignited immediately. This consequently leads to incomplete combustion and thus to a large amount of CO.

The fact that the mean value of the tests with SOC = 100 % does not clearly follow the increasing trend with higher SOC can have various causes. For example, there are many more values of fully charged cells than of partially charged cells, which increases the variance, clearly

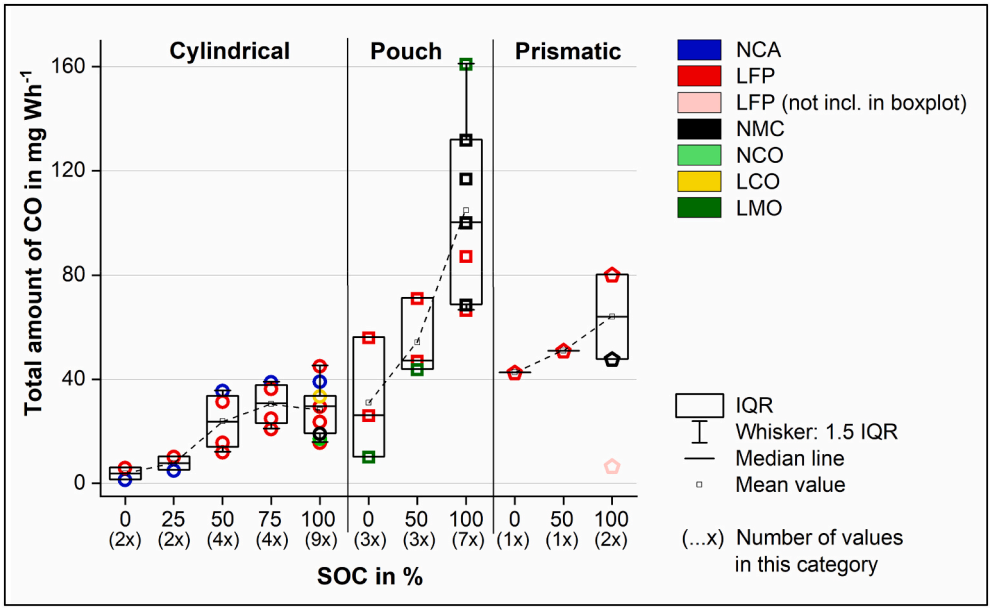

Fig. 4. CO production of cells depending on their cell geometry, SOC and cathode active material.

recognizable in the investigations on NCA cells by Golubkov et al. [15]. In addition, the increase of CO emission between a 75 % partially charged and a 100 % fully charged cell is sometimes not present at all, for which see Gully et al. [16]. Not least values of NCO and LCO cells are found only in the range of fully charged cylindrical cells. These have a comparatively low CO production and keep the average value down.

5.2.1.2. CO production of pouch cells. In the right section of Fig. 4, it can be seen that pouch cells also release more CO during a TR, the higher the SOC of the cells. This generally recognizable pattern corresponds to the findings of Ribière et al. [13], which he drew from his combustion tests on pouch cells. He recognized from the molar ratio nCO_2/nC_{total}, which in his tests assumed the values 90.0 %, 98.0 % and 99.5 % for cells with 100 %, 50 % and 0 % SOC, that the combustion efficiency decreases with the SOC of the cells. This agrees with the statement that the production of CO raises with the SOC.

Although pouch cells as well as cylindrical cells are affected by the same trend of CO release, it is noticeable that the pouch cells show a higher average CO production depending on their SOC. However, it should be mentioned that this assumption is based on only a few detectable measured values.

Furthermore, three connected series of measurements can be seen which record the CO emissions from pouch cells as a function of their SOC. These are two measurement series with LFP pouch cells using different electrolytes by Lecocq et al. [68] and one measurement series with LMO pouch cells by Ribière et al. [13]. Lecocq has concluded that for a given SOC, cells with a LiFSI-based electrolyte result in a lower CO yield than the corresponding cells containing a Lithium hexafluorophosphate (LiPF6)-based electrolyte. He also confirms that in both technologies the higher SOC favors incomplete combustion.

In the case of the LFP pouch cells, the increase in the SOC appears to have a linear relationship to the CO release, whereas in the case of the LMO pouch cells, this relationship can only be assumed to exist between 0 % and 50 %. With a SOC increase from 50 % to 100 %, CO release increases disproportionately by a factor of 4. This is presumably due to the fact that fully charged LMO cells go through much more violently than LFP cells in the same SOC. According to Lecocq's findings, oxygen consumption is so severely restricted by the sudden explosive release of energy from LMO cells that the full extent of combustion is considerably reduced.

In general, it can be said that the mean increase in CO emission values with larger SOC is clearly visible. However, a clear dependence between the tested cathode active materials and the CO release cannot be identified.

5.2.1.3. CO production of prismatic cells. The CO emission values of prismatic cells were taken from the two publications by Liu et al. [43] and Huang et al. [80]. Liu et al. [43] investigated prismatic LFP cells with a capacity of 22 Ah and different SOCs. In their experiments, they observed that the intensity of the jet fire during TR increased with the SOC. At a SOC of 100 %, the jet fire was blown out, followed by an intense emission of smoke gas. As with the other cell geometries, the CO content of the emitted smoke gases increases with the SOC.

Huang et al. [80] investigated the propagation characteristics of fully charged prismatic cells with two different cathode active materials and a significantly higher capacity during TR. Their NMC cells had a capacity of 100 Ah and their LFP cells had a similar capacity of 105 Ah. Their measured values for both cell types are much lower than those of Liu et al. The NMC cells, which had a TR with a violent jet fire and combustion behavior, released significantly more CO (48 mg Wh^{-1}) than the LFP cells. These had no flame appearance during the test, but released a considerable amount of white smoke, in which a CO level of 6 mg Wh^{-1} was measured. It can be assumed that in this case the TR was suppressed by unknown reasons. Therefore, this measured value is not considered in the boxplot.

5.2.2. Production of toxic and flammable gases

During the TR of a LIB, considerable amounts of numerous smoke gases are produced, which have an increasing importance in battery research due to their combustibility, toxicity and/or asphyxiating effect on the human organism. Thus, in recent years, a number of researcher investigated the release of such flammable and harmful gases released from LIBs in the event of a TR [13,15,18,66,76]. However, the frequency of such studies is still not high enough to allow a differentiated assessment, as was presented in chapter 5.1.2 for the CO component. Nevertheless, all recorded data on the release of the gas components CO, CO_2, HF, H_2, CH_4, NO, SO_2 and HCl can be found in a gas release table in the supplementary material of this analysis.

5.2.3. Total amount of gas emitted

The total amount of gas emitted from a cell during TR is shown in Fig. 5. This figure contains measured values of 42 tests from 8 different

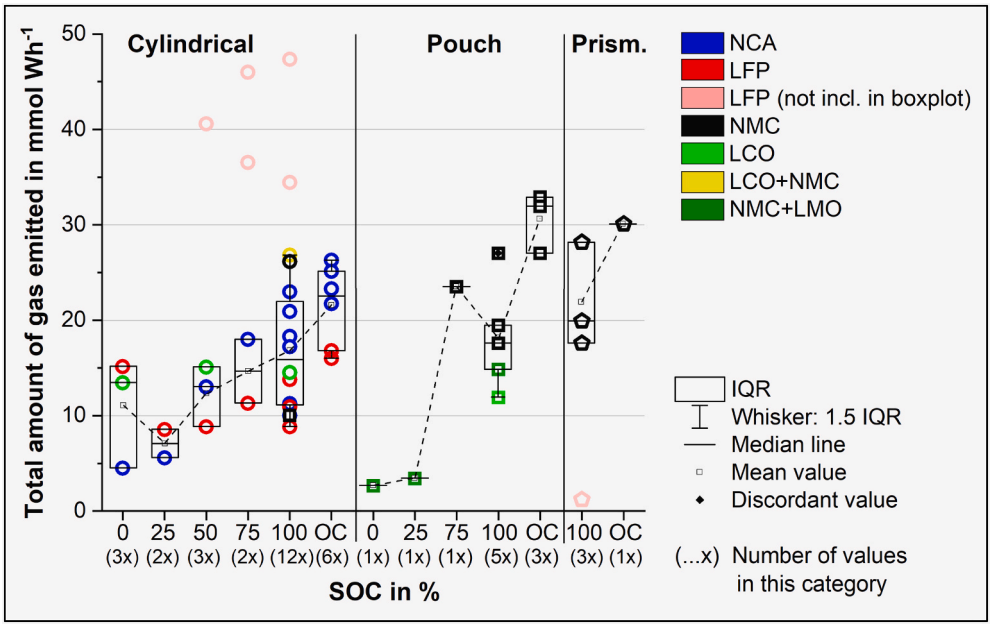

Fig. 5. Total amount of gas emitted from cells during TR as a function of cell geometry, cathode active material and SOC, including overcharge (OC) conditions.

references. The values are again subdivided according to cell design, SOC and cathode active material. Their values are normalized to the nominal energy of the batteries tested. The unit is given as mmol Wh^{-1}. Most of the data that could be found in the studies reviewed are, as already noted several times, in the range of cylindrical cell geometries. There, and just as with the pouch and prismatic cells, the fully charged cells were a preferred test pattern.

5.2.3.1. Gas emitted of cylindrical cells. During the data analysis, some values with outlier character were found. A few of them were not included in Fig. 5 for reasons of clarity, but which should not remain unmentioned here. For example, Gully et al. [16] recorded two results with comparatively high values when they examined 18,650 LFP cells. They determined 124 mmol Wh^{-1} from a fully charged cell during TR and 339 mmol Wh^{-1} from a cell that vented off under the influence of a 50 A overcharge but did not experience the temperature rise common to TR. The five values of cylindrical LFP cells, at the top of the graph (highlighted in pink) seems to be also outlier data points, found by Gully et al. [16] and by Diaz et al. [65]. No reasons could be identified for their values deviating strongly from the average. Therefore, assuming that they are outliers, they were not included in the creation of the boxplot. Based on the remaining data points, it can be seen very clearly, especially in the cylindrical area, that the amount of gas emitted increases with increasing SOC.

The investigations on 18,650 LIBs by Golubkov et al. [15] from 2015 deal to a large extent with the analysis of the released gases from LFP and NCA cells at different SOC including overcharges up to a SOC of 140 %. All cells here were made to undergo TR by thermal abuse. In 23 test runs, they found that among other things the cathode active material has a high influence on the quantity of released gases in TR conditions. However, this fact is based on the different cell capacities and the associated energy density of the cells, which they bring with them with identical construction but different cathode active materials.

Thus, when looking at Golubkov's absolute measured values of gas emission, it is noticeable that the measured amount of produced smoke gas is several times higher for 18,650 NCA cells than for 18,650 LFP cells. The gas emission of discharged and 25 % charged NCA cells is about the same respectively about two times higher than for LFP cells of the same SOC. At the SOC of 50 % or 75 %, the gas emission of NCA cells is higher by a factor of $f \approx 5$. For a fully charged cell, the factor reaches its maximum value of $f \approx 9$.

An earlier study by Golubkov et al. [14] is from 2014, where he investigated three species of 18,650 cells: LFP, NMC and LCO/NMC with 1.1, 1.5 and 2.6 Ah as a nominal capacity respectively. Of the three tested specimens, the LCO/NMC cell and the NMC cell show the highest values of vented gases in area of fully charged cylindrical cells (outlier excluded). At 14 mmol, the LFP cell has the lowest amount of gas produced among the three cell types studied, but the highest compared to LFP cells with SOC = 100 % of other studies.

Lammer et al. [77] investigated three different kinds of NCA cells. One cell type had a capacity of 3.2 Ah, the other two had a capacity of 3.5 Ah. All cell types tested between 2 and 4 times were fully charged at the time of the tests. Lammer et al. noted that all cell types exhibited the same three characteristic events (first venting, TR and cell deflagration) over the course of the tests. In addition, they note that the cell types, even those with identical cathode active material and similar capacities, exhibit drastic differences in gas emission during each characteristic event. It cannot be rejected that the reproducibility of the TR initiation mechanism or the test method play a role in the measured value deviation. However, normalized to their cell performance and placed in the context of this meta-analysis, the study results of 11.26 to 18.32 mmol Wh^{-1} fit well into the prevailing range of values of the underlying population.

Contrary to the just mentioned findings that the total amount of released gas depends essentially on the cathode active material, Roth and Orendorff [104] claim that the cathode active material has hardly any influence on it. Their measurements of the gases released from five different 18,650 cells with diverse cathode active materials during a TR showed little difference between them. Therefore, they believe that the volume of electrolyte used in the cell is the main factor influencing the volume of gas emitted. According to them, energy released during the combustion of the electrolyte is many times higher than the electrical energy stored in the cell [104].

5.2.3.2. Gas emitted of pouch and prismatic cells. Compared to the cylindrical cells, pouch and prismatic cells are rather rarely represented in the research area *Safety of LIBs*. Due to the limited amount of data available for these cell designs, the authors felt compelled to also show values in the overcharge category, which did not result from the heating of overcharged cells, but from overcharging until cell failure (see Fig. 5).

These values are taken from investigations with overcharged pouch cells by Gully et al. [16], Essl et al. [17] and from the *Handbuch Lithium-Ionen-Batterien* by Korthauer [105]. The value of the overcharged prismatic cell also comes from Essl et al. [17], who studied the effects of various TR triggers. They found that the TR caused by overcharge is more violent than a TR caused by overtemperature or nail-penetration. The overcharge triggered TR resulted in a higher amount of smoke gas and the gas components shifted towards higher volume percent of flammable, explosive and toxic gas compounds such as H_2 and CO [17].

The measured value at the bottom of the diagram originates from the experiments of Huang et al. [80], whose prismatic 105 Ah LFP cell experienced an inhibited TR and thus a barely comparable smoke gas emission. The measured value was included for the sake of completeness, but not considered in the creation of the boxplot.

5.3. LFP - the most studied cathode active material

From the data collected during the meta-analysis, LFP is the most studied cathode active material. Both in terms of heat release and smoke gas emission, numerous data can be found that were collected using cells with this cathode active material. With 85 entries out of a total of 243 experimental heat release data collected, the studies with LFP cells account for almost 35 % of the data volume. For this reason, a separate consideration of the heat release and smoke gas emission can be carried out in this section of the work exclusively for LFP cells as a function of their cell geometry and SOC. According to the available data, in the following, the heat release of LFP pouch cells, the heat release of LFP cylindrical cells and the HF released of pouch and prismatic LFP cells are picked out as three central themes.

Thus, with the aid of the extensive data available, the statistic population was sufficient to produce the diagram shown in Fig. 6, which shows the THR of LFP cells as a function of their SOC and the type of calorimeter used for the measurement. It clearly shows that the higher the SOC of the cell, the higher the heat release. This tendency is opposite to the HF gas emission from LFP cells, where with increase of the SOC the amount of HF gas emitted decreases (see Fig. 7).

5.3.1.1. Heat release of LFP pouch cells. Measurements of heat release from LFP cells as a function of their SOC were often performed with cylindrical cells. Only two of the sources investigated used pouch cells for this purpose. These are Sturk et al. [59] and Peng et al. [49].

Sturk et al. [59] found that the total amount of electrical energy stored in the cells has no significant effect on the total amount of thermal energy released. However, it is likely that there is a nonlinear relationship between the SOC and the HRR. Accordingly, the LFP pouch cells show in the experiments of Sturk et al. that medium and high states of charge (SOC = 50–100 %) result in higher PHRR than low states of charge (SOC = 0–25 %). From the dependence on SOC, they conclude that the electrical energy content of a cell contributes to the onset of the TR by providing the activation energy required to initiate TR. The importance of electrical energy as a trigger of TR appears to be less for medium to low SOC than for fully charged cells. Sturk et al. interpret their data to mean that for LFP cells below 75 % SOC, the dependence on SOC is less significant [59].

Peng et al. [49], who evaluated the fire hazard of LFP pouch cells based on various parameters such as ignition time, surface temperature, PHRR, THR, mass loss and flame size, came to similar conclusions from their results. They concluded that the intensity of combustion increases with increasing SOC, but not only flame height and PHRR but also THR increase significantly.

5.3.1.2. Heat release of cylindrical LFP cells. Six publications deal with the investigation of cylindrical cells of the 18,650 type. The majority of the measured data yields graphs that show a greater heat release as the SOC of the tested cells increases. Publications [28,31] are from Chen et al. and describe tests with 18,650 LFP cells (LCO cells were investigated too, but are not discussed in this section for thematic reasons). The experimental values of the LFP cells were included in Fig. 6. Chen et al. [28] noticed that with increasing SOC the maximum surface temperature of the cell, mass loss, HRR and THR increase. Beside the key findings Chen et al. found in [28] that both tested cell types have two ejection fires which are mainly caused by the oxygen releasing reactions during TR. Their experiment results demonstrate that with increasing SOC the time to the first ejection and the time gap between first and second ejection decreases, while the ejection temperature increase with that. Therefore, they conclude that LIBs with high SOC are more dangerous than less charged LIBs. They attribute this difference to the distribution of the lithium ions stored in the cell.

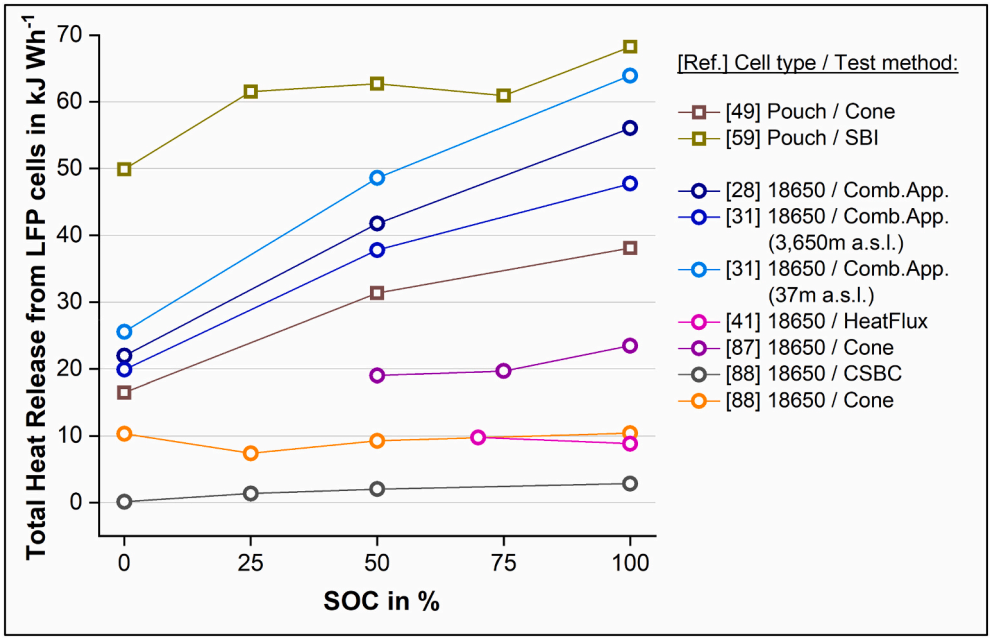

Fig. 6. Total Heat Release of LFP cells as a function of cell geometry and SOC.

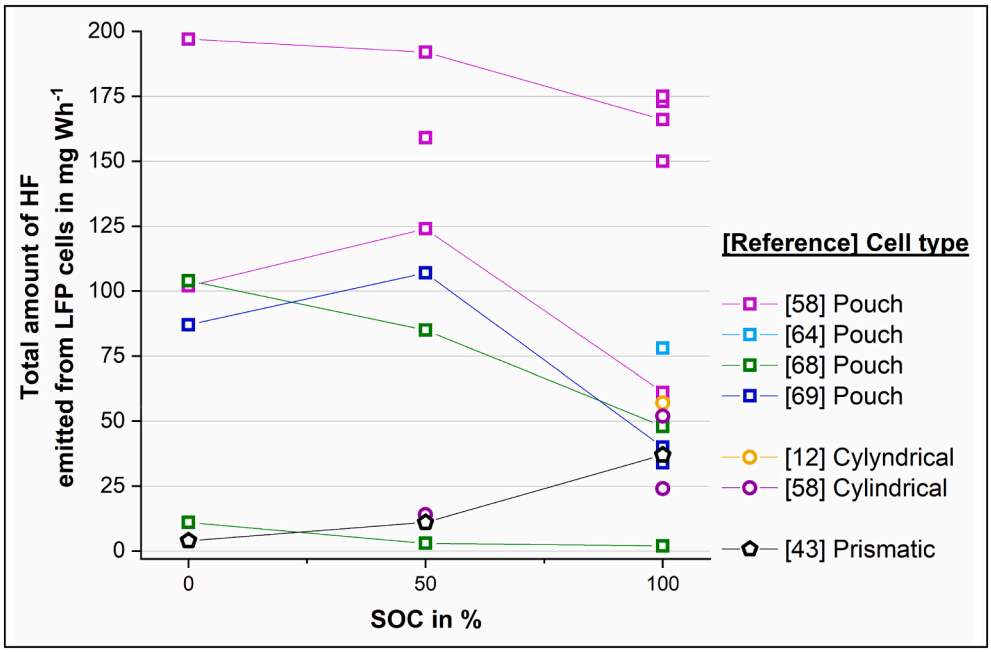

Fig. 7. HF released from LFP cells as a function of cell geometry and SOC.

In [31], Chen et al. elaborate on their findings and address the influence of ambient air pressure on the intensity of the effects occurring during a TR. With their investigation results from laboratories in Hefei (37 m above sea level), and in Lhasa (3650 m above sea level), they postulate that the environmental pressure has significant impact on the combustion heat. They found that the THR values of LIBs at $p_a = 100.8$ kPa (tested in Hefei) are significantly higher than that at $p_a = 64.3$ kPa (tested in Lhasa). Their key finding is that the batteries at high environmental pressure have a greater unit growth rate of combustion heat for every 1 % increase in SOC.

Two of the publications considered are by Ouyang et al. In [87], they investigate the heat release of cylindrical LFP cells brought to TR with an electric heater using the oxygen consumption method. In [41], they use a similar experimental setup for the same cell type but record the heat release using a heat flux radiometer. The THR values recorded from this publication are the only graph entries that are lower at a SOC of 100 % than at a lower SOC, which may be due to the difficult alignment for accurate measurement on the small battery surface and the cross-sensitivity of a heat flux sensor.

5.3.1.3. HF released of LFP cells. It is known that HF has an extremely high acute hazard potential. Absorbed through the respiratory tract or skin, HF has a highly damaging effect on all contacted tissues [106,107]. Because LFP cells have been studied so frequently, there is also a good amount of data available on HF release during TR of this cell type.

The collected HF readings of cylindrical cells and pouch cells as a function of their SOC are shown in Fig. 7. Values that are part of continuous series of measurements are connected with a line. In this diagram, it can be seen that fully charged LFP pouch cells release a smaller amount of HF during TR than discharged LFP cells in most cases. One possible explanation is that higher SOC is associated with higher reaction temperatures during TR, which causes the generated HF to decompose and/or react to other fluorine-containing compounds, making the HF gas undetectable. In the test series by Lecocq et al. [68], there is a tendency for HF production to decrease with increasing SOC. In contrast, in the test series of Andersson et al. [69], the decreasing HF release with increasing SOC is interrupted by a peak at a SOC of 50 %. Unlike many other studies on cylindrical cells, Andersson et al. do not deal with 18,650 or 21,700 cells, but with 26,650 cells. However, the above-mentioned peculiarity in the HF curve cannot be attributed to the cell design, because Larsson et al. [58] even record both characteristic curve shapes within one measurement campaign during their investigations on LFP pouch cells. All three research groups used an FTIR spectrometer for their measurements.

In addition to the turbulent gas emission, which poses a challenge for reproducible detection of the gases, various reasons for deviating HF curves are given in the test results. For example, it was found that HF components from the sample gas are adsorbed in the FTIR filter and thus do not enter the measurement cell [108]. Larsson et al. [58] also note that HF was temporarily clogged in the sampling system during their measurements. However, the test method is not the only reason for different measured values.

The flammable electrolyte in a LIB usually contains $LiPF_6$ or other fluorine-containing lithium salts. Fluorine-containing compounds can also be found in other parts of the LIB. For example, many LIBs use polyvinylidene fluoride (PVDF) as a binder for the chemically active substances in the electrodes. Fluorophosphates [109,110] are also used in the flame retardants in the electrolyte and separator [111] and in various additives. Depending on the cell temperature during TR, these fluorine-containing components eventually volatilize out of the battery cells. [58]. It is also possible that some of the fluorine remains in the cell and forms other compounds there [66]. At elevated temperatures the fluorine content released from the cell can form gases such as HF, phosphorus pentafluoride (PF_5) and phosphoryl fluoride (POF_3) [58]. As an example, the reaction equations according to Yang et al. [67] and Kawamura et al. [112] can be used for the decomposition of $LiPF_6$. Wilken et al. [113] confirm in their investigations on the thermal decomposition of $LiPF_6$-based LIB electrolytes that the decomposition of $LiPF_6$ follows the path of pyrolysis of the salt. PF_5 is formed first, which reacts in the next step with external moisture or cell internal moisture contamination to HF (see Eqs. (3)–(4)).

$$LiPF_6 \rightarrow LiF + PF_5 \quad (4)$$

$$PF_5 + H_2O \rightarrow POF_3 + 2HF \quad (5)$$

$$LiPF_6 + H_2O \rightarrow LiF + POF_3 + 2HF \quad (6)$$

Sturk et al. [64] found that the concentration of HF in gases released

from LFP cells is more than an order of magnitude higher than for cells with NMC/LMO cathodes. From this, they conclude that the formation of HF is favoured when TR develops over a longer period of time, as it is mostly the case with LFP cells. According to Hammami et al. [114] and Sun et al. [115], the catalyzing effect of nickel and manganese in the NMC/LMO cells is crucial for the low HF concentration in the released gases.

Diaz et al. [65] conclude that the gas composition of thermally abused batteries varies with its SOC. Accordingly, HF is more stable at low SOC than at high SOC, where formation of other undetected fluorides such as tetrafluoromethanes (CF_4) may occur. This observation is consistent with previously published work by Ribière et al. [13] and Lecocq et al. [68].

Liu et al. [43] published their study results on prismatic 22 Ah LFP cells, which they brought to TR by overheating. Among the publications found on this topic, they are the only ones to report an increasing HF emission with increasing SOC. They explain this by large amounts of electrolyte released during mechanical cell failure, which reacts with the ambient air to form HF. According to their observations, the amount of electrolyte released is much greater at high SOC than at low SOC due to the higher vent pressure, since more of the electrolyte bound in the cell is emitted at high pressures.

6. Conclusion

The objective of this meta-analysis was to determine whether the gas and heat release hazards posed by lithium-ion batteries during thermal runaway could be quantified and differentiated with respect to cell geometry and cathode active material. Based on a quantitative and qualitative analysis of 135 scientific papers (including papers that do not contain specific quantitative data) on these two focal points, it can be concluded that, on the basis of the available data, the determination of a hazard potential of lithium-ion batteries differentiated by cell type is very complex and relatively coarse-meshed. Despite the large number of published studies, there are only a few mutually comparable measured values. The analysis of the data has shown that with the most frequently investigated

- cell geometries (cylindrical, pouch, prismatic),
- cathode active materials (Lithium Iron Phosphate, Lithium Nickel Manganese cobalt Oxide, Lithium Nickel Cobalt Aluminium, Lithium Manganese Oxide, Lithium Cobalt Oxide),
- states of charge (0 %, 50 %, 100 %),
- initiation methods (electric heating, radiant heating, fire heating) and
- TEST methods for the determination of heat release (single burning item apparatus, combustion apparatus, cone calorimeter, accelerating rate calorimeter) respectively
- test methods for the determination of smoke gas emission (Fourier transform infrared spectroscopy, gas chromatography - mass spectrometry, paramagnetic analyzer, multi-gas analyzer)

alone, there are 18 parameter variations that have a significant effect on the heat release and smoke gas emission values to be analyzed. In addition, there is the number of cells per test and their nominal energy. Both factors are calculated against the measured values in this analysis, so that standardized and easily comparable results can be given.

Nevertheless, conclusions can be drawn from the analysis to estimate the maximum expected impact of particular battery types during thermal runaway. The more closely examined values show that a 100 % charged LIB can produce a peak heat release rate of 1.8 kW Wh^{-1} for cylindrical cells, 2.6 kW Wh^{-1} for pouch cells and 2.8 kW Wh^{-1} for prismatic cells in the event of a thermal runaway (see Fig. 2). The highest values of total heat release are 63 kJ Wh^{-1} for cylindrical cells, 71 kJ Wh^{-1} for pouch cells and 112 kJ Wh^{-1} for prismatic cells (see Fig. 3). Probably, the percentage of the housing material has an impact here, as this incombustible part is mainly higher for cylindrical cells. Since the heat release values increase with increasing state of charge, cells with lower states of charge pose a lower risk from released heat. Differentiation of the values on the basis of the underlying cathode active materials of the cells is not possible due to the large number of calorimeter types used and the associated influences on the measured values.

By analyzing the smoke gas emission, this work has shown that 100 % charged cylindrical lithium-ion batteries release a likely smoke gas quantity of up to 27 mmol Wh^{-1} during the thermal runaway (see Fig. 5). Individual, unverifiable measurements even yield values of up to 48 mmol Wh^{-1}. For pouch and prismatic cells, the total smoke gas emission is 30 mmol Wh^{-1} and 33 mmol Wh^{-1}, respectively. The results also provide insight into the CO production of lithium-ion batteries. The maximum measured values for cylindrical cells are 45 mg Wh^{-1} and for pouch cells 161 mg Wh^{-1} (see Fig. 4). In both categories, the measured values increase with increasing state of charge. In addition, the cathode active materials Lithium Nickel Manganese Cobalt Oxide and Lithium Nickel Cobalt Aluminium are frequently found among the higher measured values. The analysis of the released HF gas quantities showed that the detected HF content decreases with increasing state of charge of the cells. Here, the highest value of 197 mg Wh^{-1} is achieved by a pouch cell with 0 % state of charge. The highest value resulting from a 100 % charged pouch cell is 175 mg Wh^{-1} (see Fig. 7). It turned out that the fluorine content from fully charged cells also enters other fluorine-containing compounds and is therefore no longer available for the formation of HF.

The initial hypotheses were largely confirmed in the course of the meta-analysis. Based on the collected data, it could be shown that the cathode active material influences the heat release of cells at 100 % state of charge during thermal runaway. The normalized heat release of cells with different cathode active materials can be clearly differentiated in the diagrams. It should be noted, however, that a value normalization in terms of cell weight, instead of in terms of nominal energy, would rank the heat release values of different cathode active materials differently. However, such a normalization is hardly possible due to very often missing weight data. The influence of the cathode active material on the gas emission of cells during thermal runaway cannot be clearly determined from the data collected.

The influence of cell geometry on heat release and gas emission of cells during thermal runaway can be clearly determined. On average, pouch cells achieve the highest values for both heat release and gas emission. Significantly lower values are achieved by prismatic cells. The cylindrical cells show the lowest emissions. The evaluations of Carbon Monoxide and hydrogen fluoride release are also clearly characterized by the high emission values of the pouch cells.

The influence of the different methods used to initiate the thermal runaway in the studies reviewed cannot be quantified within the scope of this analysis. It is clear, however, that the initiation methods included in this study, e.g. electric heating, radiant heating or fire heating, are affecting the quantities of heat release and smoke gas emission differently, due to their different energy inputs. It turns out that higher energy input increases the measured values of heat release and gas emission.

The main challenge for the preparation of this meta-analysis was the diversity of the test methods, which can be assumed to limit the comparability of the data due to their different initial parameters, such as ignition source, ignition energy, ambient conditions, measuring method, measuring point, etc. The studies analyzed in this paper each use a total of 10 different methods to determine the heat release and gas emission. The influence of these test methods on the values of heat release and gas emission is not quantifiable but can be seen to some extent in the graphs shown. Especially for the measured values of the peak heat release rate, a certain method-dependent distribution of the values in the measurement range is recognizable.

To date, no scientific paper has been published that examines the same cell type with different test methods, thus disproving this

assumption. It is evident that for a higher comparability and for more precise conclusions, a standard test method is needed describing the test rig, a defined test procedure and all parameters including the detailed material composition of investigated cell types.

Once having a standard makes it possible to compare results quantitively. Research institutions should work together, for example in performing round robin tests. This can be the basis for standardized tests and therefore comparable data and robust statements. In conclusion, this would lead to a better understanding of the various available and next generations of LIB and therefore be an important step for the safety and usage of LIB.

A full list of all recorded measurement values with associated information on the test conditions will be published together with this meta-analysis.

Funding

This research did not receive any specific grant from funding agencies in the public, commercial, or not-for-profit sectors.

Declaration of competing interest

The authors declare that they have no known competing financial interests or personal relationships that could have appeared to influence the work reported in this paper.

Data availability

The authors analyze data collected by other authors. These data are available in the supplementary Materials.

Appendix A. Supplementary data

Supplementary data to this article can be found online at https://doi.org/10.1016/j.est.2022.106579.

References

[1] M. Ghiji, S. Edmonds, K. Moinuddin, A review of experimental and numerical studies of lithium ion battery fires, Appl. Sci. 11 (1247) (2021) 29.
[2] X. Feng, et al., Characterization of penetration induced thermal runaway propagation process within a large format lithium ion battery module, J. Power Sources 275 (2015) 261–273.
[3] Q. Wang, et al., Thermal runaway caused fire and explosion of lithium ion battery, J. Power Sources 208 (2012) 210–224.
[4] X. Feng, et al., Thermal runaway features of large format prismatic lithium ion battery using extended volume accelerating rate calorimetry, J. Power Sources 255 (2014) 294–301.
[5] M. Börner, et al., Correlation of aging and thermal stability of commercial 18650-type lithium ion batteries, J. Power Sources 342 (2017) 382–392.
[6] R. Spotnitz, J. Franklin, Abuse behavior of high-power, lithium-ion cells, J. Power Sources 113 (2002) 81–100.
[7] E. Rahimzei, K. Sann, M. Vogel, Kompendium: Li-Ionen-Batterien - Grundlagen, Bewertungskriterien, Gesetze und Normen, in: VDE Verband der Elektrotechnik Elektronik Informationstechnik e. V, 2015.
[8] G.G. Eshetu, et al., Fire behavior of carbonates-based electrolytes used in Li-ion rechargeable batteries with a focus on the role of the LiPF6 and LiFSI salts, J. Power Sources 269 (2014) 804–811.
[9] L. Chancelier, et al., Targeting adequate thermal stability and fire safety in selecting ionic liquid-based electrolytes for energy storage, Phys. Chem. Chem. Phys. 16 (2014) 1967–1976.
[10] J. Tübke, J. Vogt, in: J. Garche, K. Brandt (Eds.), Li-Battery Safety. Electrochemical Power Sources: Fundamentals, Systems, and Applications, Elsevier, 2018, p. 670.
[11] L. Rong, X. Cheng, Y. Fu, in: Effect of States of Charge on the Burning Behaviors of Lithium Ion Batteries, 2020, p. 5.
[12] F. Larsson, et al., in: Gas Emissions from Lithium-Ion Battery Cells Undergoing Abuse from External Fire SP Technical Research Institute of Sweden, 2016, p. 5.
[13] P. Ribière, et al., Investigation on the fire-induced hazards of Li-ion battery cells by fire calorimetry, Energy Environ. Sci. 5 (2012) 5271–5280.
[14] A.W. Golubkov, et al., Thermal-runaway experiments on consumer Li-ion batteries with metal-oxide and olivin-type cathodes, RSC Adv. 4 (2014) 3633–3642.
[15] A.W. Golubkov, et al., Thermal runaway of commercial 18650 Li-ion batteries with LFP and NCA cathodes – impact of state of charge and overcharge, RSC Adv. 5 (2015) 57171–57186.
[16] B. Gully, et al., in: Technical Reference for Li-ion Battery Explosion Risk and Fire Suppression, DNV-GL, 2019, p. 202.
[17] C. Essl, A.W. Golubkov, A. Fuchs, Comparing different thermal runaway triggers for two automotive lithium-ion battery cell types, J. Electrochem. Soc. 167 (2020) 14.
[18] M. Lammer, et al., Influence of aging on the heat and gas emissions from commercial lithium ion cells in case of thermal failure, Electrochem. Sci. Eng. 8 (1) (2018) 10.
[19] Acute Exposure Guideline Levels, US Environmental Protection Agency, Office of Pollution Prevention and Toxics, Washington, 2021. https://www.epa.gov/aegl/access-acute-exposure-guideline-levels-aegls-values#chemicals.
[20] Immediately Dangerous To Life or Health, The National Institute for Occupational Safety and Health, 2018. https://www.cdc.gov/niosh/idlh/intridl4.html.
[21] 2019 ERPG/WEEL Handbook, American Industrial Hygiene Association (AIHA), 2019. Hyattsville, USA.
[22] M. Chen, C. DeZhou, J. Wang, Experimental study on the combustion characteristics of primary lithium batteries fire, Fire. Technol 52 (2016) 365–385.
[23] P. Huang, et al., Experimental and modeling analysis of thermal runaway propagation over the large format energy storage battery module with Li4Ti5O12 anode, Appl. Energy 183 (2016) 659–673.
[24] Q. Wang, et al., Combustion behavior of lithium iron phosphate battery induced by external heat radiation, J. Loss Prev. Process Ind. 49 (2016) 961–969.
[25] P. Ping, et al., Study of the fire behavior of high-energy lithium-ion batteries with full-scale burning test, J. Power Sources 285 (2015) 80–89.
[26] P. Huang, et al., The combustion behavior of large scale lithium titanate battery, Sci. Rep. 5 (2014) 1–12.
[27] Y. Peng, et al., A comprehensive investigation on the thermal and toxic hazards of large format lithium-ion batteries with LiFePO4 cathode, J. Hazard. Mater. 381 (2020).
[28] M. Chen, et al., Investigation on the thermal hazards of 18650 lithium ion batteries by fire calorimeter, J. Therm. Anal. Calorim. 122 (2015) 755–763.
[29] M. Chen, et al., Experimental investigation on the effect of ambient pressure on thermal runaway and fire behaviors of lithium-ion batteries, Int. J. Energy Res. 43 (2019) 4898–4911.
[30] M. Chen, et al., Effects of heat treatment and SOC on fire behaviors of lithium-ion batteries pack, J. Therm. Anal. Calorim. 136 (2019) 2429–2437.
[31] M. Chen, et al., Environmental pressure effects on thermal runaway and fire behaviors of lithium-ion battery with different cathodes and state of charge, Process Saf. Environ. Prot. 130 (2019) 250–256.
[32] Z. Wang, et al., Thermal runaway and fire behaviors of large-scale lithium ion batteries with different heating methods, J. Hazard. Mater. 379 (2019).
[33] ASTM International, ASTM E1981-22, in: Standard Guide for Assessing Thermal Stability of Materials by Methods of Accelerating Rate Calorimetry, 2020, p. 8.
[34] J. Ye, et al., Thermal behavior and failure mechanism of lithium ion cells during overcharge under adiabatic conditions, Appl. Energy 182 (2016) 464–474.
[35] R. Venkatachalapathy, et al., Thermal investigations of transitional metal oxide cathodes in Li-ion cells, Electrochem. Commun. 2 (2000) 104–107.
[36] S. Zheng, et al., Probing the heat sources during thermal runaway process by thermal analysis of different battery chemistries, J. Power Sources 378 (2018) 527–536.
[37] C. Zhao, J. Sun, Q. Wang, Thermal runaway hazards investigation on 18650 lithium-ion battery using extended volume accelerating rate calorimeter, J. Energy Storage (2020) 28.
[38] ASTM International, n.d. ASTM D2015-85 - Standard Test Method for Gross Calorific Value of Coal and Coke by the Adiabatic Bomb Calorimeter: p. 11.
[39] R.E. Lyon, R.N. Walters, Energetics of lithium ion battery failure, J. Hazard. Mater. 318 (2016) 164–172.
[40] ASTM International, ASTM E2684-17 - Standard Test Method for Measuring Heat Flux Using Surface-mounted One-dimensional Flat Gages: n.d. p. 7.
[41] D. Ouyang, et al., Investigation into the fire hazards of lithium-ion batteries under overcharging, Appl. Sci. 7 (2017).
[42] International Organization for Standardization, n.d. ISO 9705-1:2016-02 - Reaction to Fire Tests - Room Corner Test for Wall and Ceiling Lining Products - Part 1: Test Method for a Small Room Configuration: p. 42.
[43] P. Liu, et al., Thermal runaway and fire behaviors of lithium iron phosphate battery induced by over heating, J. Energy Storage 31 (2020) 13.
[44] O. Willstrand, et al., Toxic gases from fire in electric vehicles, in: Safety & Transport, Safety Research, Research Institutes of Sweden, 2020.
[45] International Organization for Standardization, ISO 5660-1:2015-03 - Reaction to Fire Tests - Heat Release, Smoke Production and Mass Loss Rate - Part 1: Heat Release Rate (Cone Calorimeter Method) and Smoke Production Rate (Dynamic Measurement): n.d. p. 55.
[46] Z. Wang, et al., Fire behavior of lithium-ion battery with different states of charge induced by high incident heat fluxes, J. Therm. Anal. Calorim. (2018), https://doi.org/10.1007/s10973-018-7899-y. Published online: 08 November 2018.
[47] D. Ouyang, M. Chen, J. Wang, Fire behaviors study on 18650 batteries pack using a cone-calorimeter, J. Therm. Anal. Calorim. 136 (2019) 2281–2294.
[48] G. Zhong, et al., Thermal runaway and fire behavior investigation of lithium ion batteries using modified cone calorimeter, J. Therm. Anal. Calorim. 135 (2019) 2879–2889.
[49] Y. Peng, et al., A new exploration of the fire behaviors of large format lithium ion battery, J. Therm. Anal. Calorim. 139 (2020) 1243–1254.

[50] A.O. Said, et al., Simultaneous measurement of multiple thermal hazards associated with a failure of prismatic lithium ion battery, Proceedings of the Combustion Institute 37 (2019) 4173–4180.
[51] International Organization for Standardization, DIN EN ISO 11357-1:2017-02 - Plastics - Differential Scanning Calorimetry (DSC) - Part 1: General Principles: n. d. p. 42.
[52] Y.S. Duh, M.T. Tsai, C.S. Kao, Characterization on the thermal runaway of commercial 18650 lithium-ion batteries used in electric vehicle, J. Therm. Anal. Calorim. 127 (2017) 983–993.
[53] C.Y. Jhu, et al., Thermal explosion hazards on 18650 lithium ion batteries with a VSP2 adiabatic calorimeter, J. Hazard. Mater. 192 (2011) 99–107.
[54] C.Y. Jhu, et al., Thermal runaway potential of LiCoO2 and Li(Ni1/3Co1/3Mn1/3)O2 batteries determined with adiabatic calorimetry methodology, Appl. Energy 100 (2012) 127–131.
[55] Deutsche Institut für Normung E. V. , DIN EN 13823:2020-09 - Reaction to Fire Tests for Building Products - Building Products Excluding Floorings Exposed to the Thermal Attack by a Single Burning Item: n.d. p. 115.
[56] F. Larsson, et al., Characteristics of lithium-ion batteries during fire tests, J. Power Sources 271 (2014) 414–420.
[57] F. Larsson, P. Andersson, B.E. Mellander, Lithium-ion battery aspects on fires in electrified vehicles on the basis of experimental abuse tests, MDPI Batteries (2016) 2.
[58] F. Larsson, et al., Toxic fluoride gas emissions from lithium-ion battery fires, Sci. Rep. 7 (2017) 1–13.
[59] D. Sturk, L. Hoffmann, A.A. Tidblad, Fire tests on E-vehicle battery cells and packs, Traffic Injury Prevent. 16 (2015) 159–164.
[60] International Organization for Standardization, , ISO 12136:2011-08 - Reaction to Fire Tests - Measurement of Material Properties Using a Fire Propagation Apparatus: n.d. p. 47.
[61] ASTM International, ASTM E2058-19 - Standard Test Methods for Measurement of Material Flammability Using a Fire Propagation Apparatus (FPA): n.d. p. 30.
[62] National Fire Protection Association, NFPA 287:2017 - Standard Test Methods for Measurement of Flammability of Materials in Cleanrooms Using a Fire Propagation Apparatus (FPA): n.d. p.
[63] International Organization for Standardization, ISO 19702:2015-08 - Guidance for Sampling and Analysis of Toxic Gases and Vapours in Fire Effluents Using Fourier Transform Infrared (FTIR) Spectroscopy: n.d. p. 67.
[64] D. Sturk, et al., Analysis of li-ion battery gases vented in an inert atmosphere thermal test chamber, MDPI Batteries 5 (61) (2019) 17.
[65] F. Diaz, et al., Gas generation measurement and evaluation during mechanical processing and thermal treatment of spent li-ion batteries, Waste Manag. 84 (2019) 10.
[66] C. Essl, et al., Comprehensive Hazard analysis of failing automotive lithium-ion batteries in overtemperature experiments, MDPI Batteries (2020) 28.
[67] H. Yang, G.V. Zhuang, P.N. Ross Jr, Thermal stability of LiPF6 salt and li-ion battery electrolytes containing LiPF6, J. Power Sources 161 (2006) 8.
[68] A. Lecocq, et al., Scenario-based prediction of li-ion batteries fire-induced toxicity, J. Power Sources 316 (2016) 10.
[69] P. Andersson, et al., Investigation of fire emissions from Li-ion batteries, SP Technical Research Institute of Sweden, 2013.
[70] D.J. Robles, J. Jeevarajan, Fire and Gas Characterization Studies for Lithium ion Cells and Batteries, NASA Aerospace Battery Workshop, 2020.
[71] ASTM International, ASTM D4626-95, in: Standard Practice for Calculation of Gas Chromatographic Response Factors, 2019, p. 3.
[72] ASTM International, ASTM D6420-18 - Standard Test Method for Determination of Gaseous Organic Compounds by Direct Interface Gas Chromatography-Mass Spectrometry: n.d. p. 7.
[73] S. Chen, et al., Lower explosion limit of the vented gases from Li-ion batteries thermal runaway in high temperature condition, J. Loss Prev. Process Ind. 63 (2020) 7.
[74] C.J. Orendorff, et al., Quantification of lithium-ion cell thermal runaway energetics, in: Sandia Report, 2016, p. 49.
[75] A. Nedjalkov, et al., Toxic gas emissions from damaged lithium ion Batteries—Analysis and safety enhancement solution, MDPI Batteries, 2016.
[76] T. Maloney, in: Lithium Battery Thermal Runaway Vent Gas Analysis, 2016, p. 35.
[77] M. Lammer, A. Königseder, V. Hacker, Holistic methodology for characterisation of the thermally induced failure of commercially available 18650 lithium ion cells, RSC Adv. 7 (2017) 5.
[78] ASTM International, ASTM D4327-17 - Standard Test Method for Anions in Water by Suppressed Ion Chromatography: n.d. p. 13.
[79] Z. Wang, et al., Study on the fire risk associated with a failure of large-scale commercial LiFePO4/graphite and LiNixCoyMn1-x-yO2/graphite batteries, Energy Sci. Eng. 7 (2019) 9.
[80] Z. Huang, et al., Experimental investigation on thermal runaway propagation of large format lithium ion battery modules with two cathodes, Int. J. Heat Mass Transf. 172 (2021) 14.
[81] ASTM International, ASTM D3162-12 - Standard Test Method for Carbon Monoxide in the Atmosphere (Continuous Measurement by Nondispersive Infrared Spectrometry): n.d. p. 7.
[82] T. Cai, et al., Detection of Li-ion battery failure and venting with carbon dioxide sensors, eTransportation 7 (2021) (2020), 100100, p. 11.
[83] International Electrotechnical Commission, IEC 61207-3:2019 - Gas Analyzers - Expression of Performance - Part 3: Paramagnetic Oxygen Analysers: n.d.p. 58.
[84] ASTM International, n.d. ASTM D2425-21 - Standard Test Method for Hydrocarbon Types in Middle Distillates by Mass Spectrometry: p. 15.
[85] P. Andersson, et al., Using fourier transform infrared spectroscopy to determine toxic gases in fires with lithium-ion batteries, Fire Mater. 40 (999–1015) (2016) 17.
[86] P. Andersson, et al., Using Fourier transform infrared spectroscopy to determine toxic gases in fires with lithium-ion batteries, Fire Mater. 40 (999–1015) (2016) 17.
[87] D. Ouyang, et al., Experimental study on the thermal behaviors of lithium-ion batteries under discharge and overcharge conditions, J. Therm. Anal. Calorim. 132 (2018) 65–75.
[88] X. Liu, et al., Heat release during thermally-induced failure of a lithium ion battery: impact of cathode composition, Fire Saf. J. 85 (2016) 10–22.
[89] X. Liu, et al., Comprehensive calorimetry of the thermally-induced failure of a lithium ion battery, J. Power Sources 280 (2015) 516–525.
[90] A.O. Said, et al., Comprehensive analysis of dynamics and hazards associated with cascading failure in 18650 lithium ion cell arrays, Appl. Energy 248 (2019) 415–428.
[91] H. Biteau, N. Nava, Transportation of Li-ion batteries: the state of charge parameter, in: International Conference on Automatic Fire Detection & Suppression, Detection and Signaling Research and Applications Conference, 2017. Hyattsville, USA.
[92] Y. Fu, et al., An experimental study on burning behaviors of 18650 lithium ion batteries using a cone calorimeter, J. Power Sources 273 (2015) 216–222.
[93] C. Lam, et al., Full-scale fire testing of electric and internal combustion engine vehicles, in: P. Andersson, B. Sundström (Eds.), Fires in Vehicles, 2016, pp. 95–106. Baltimore, USA.
[94] P. Ping, et al., Characterization of behaviour and hazards of fire and deflagration for high-energy Li-ion cells by over-heating, J. Power Sources 398 (2018) 55–66.
[95] Y. Miao, et al., Current li-ion battery Technologies in Electric Vehicles and Opportunities for advancements, MDPI Energies 12 (1074) (2019) 20.
[96] M.A. Hannan, et al., State-of-the-art and energy management system of lithium-ion batteries in electric vehicle applications: issues and recommendations, IEEE Access 6 (2015) 19362–19378.
[97] J. Heydecke, White Paper - Einführung in die Lithium-PolymerBatterie-Technologie, Jauch Quartz GmbH & Jauch Battery Solutions GmbH, Villingen-Schwenningen, Germany, 2018. https://www.jauch.com/downloadfile/5c503f110f073193e5348d559b75424dc/.
[98] Y. Chen, et al., A review of lithium-ion battery safety concerns: the issues, strategies, and testing standards, J. Energy Chemistry 59 (2021) 83–99.
[99] Q. Huang, M. Yan, Z. Jiang, Thermal study of organic electrolytes with fully charged cathodic materials of lithium-ion batteries, J. Solid State Electrochem. 12 (2008) 671–678.
[100] Q. Wang, et al., Micro calorimeter study on the thermal stability of lithium-ion battery electrolytes, J. Loss Prev. Process Ind. 19 (6) (2006) 561–569.
[101] A. Xiao, W. Li, B.L. Lucht, Thermal reactions of mesocarbon microbead (MCMB) particles in LiPF6-based electrolyte, J. Power Sources 162 (2) (2006) 1282–1288.
[102] GESTIS-Stoffdatenbank: Kohlenmonoxid, Deutsche Gesetzliche Unfallversicherung: Berlin, Germany, 2021. https://gestis.dguv.de/data?name=001110.
[103] Z. Wang, et al., Evaluating the thermal failure risk of large-format lithium-ion batteries using a cone calorimeter, J. Fire Sci. 37 (2018) 15.
[104] E.P. Roth, C.J. Orendorff, How electrolytes influence battery safety, TheElectrochemical Society Interface (2012) 21.
[105] R. Korthauer, Handbuch Lithium-Ionen-Batterien, 2013.
[106] The National Institute for Occupational Safety and Health of HF, The National Institute for Occupational Safety and Health (NOISH), 1994. https://www.cdc.gov/niosh/idlh/7664393.html.
[107] GESTIS-Stoffdatenbank: Fluorwasserstoff, wasserfrei, Deutsche Gesetzliche Unfallversicherung, Berlin, Germany, 2021. https://gestis.dguv.de/data?name=001040.
[108] International Organization for Standardization, I.S.O.19702:2015, in: Toxicity testing of fire effluents - Guidance for analysis of gases and vapours in fire effluents using FTIR gas analysis, 2006, p. 34.
[109] Y.-U. Park, et al., Tailoring a fluorophosphate as a novel 4 V cathode for lithium-ion batteries, Sci. Rep. 2 (2012), 704.
[110] G.F. Ortiz, et al., Enhancing the energy density of safer Li-ion batteries by combining high-voltage lithium cobalt fluorophosphate cathodes and nanostructured titania anodes, Sci. Rep. 6 (2016), 20656.
[111] K. Liu, et al., Electrospun core-shell microfiber separator with thermal-triggered flame-retardant properties for lithium-ion batteries, ScienceAdvances 3 (1) (2017).
[112] T. Kawamura, S. Okada, J.-I. Yamaki, Decomposition reaction of LiPF6-based electrolytes for lithium ion cells, J. Power Sources 156 (2) (2006) 547–554.
[113] S. Wilken, et al., Initial stages of thermal decomposition of LiPF6-based lithium ion battery electrolytes by detailed Raman and NMR spectroscopy, RSC Adv. 3 (2013) 16359–16364.
[114] A. Hammami, N. Raymond, M. Armand, Lithium-ion batteries: runaway risk of forming toxic compounds, Nature 424 (2003) 635–636.
[115] J. Sun, et al., Toxicity, a serious concern of thermal runaway from commercial Li-ion battery, Nano Energy 27 (2016) 313–319.